Energy & Environmental Science

Accepted Manuscript

This article can be cited before page numbers have been issued, to do this please use: Z. Wei, K. Yan, H. Chen, Y. Yi, T. Zhang, X. long, J. Li, L. Zhang, J. Wang and S. Yang, *Energy Environ. Sci.*, 2014, DOI: 10.1039/C4EE01983K.

ROYAL SOCIETY OF CHEMISTRY

www.rsc.org/ees

View Article Online
DOI: 10.1039/C4EE01983K

Journal Name

RSCPublishing

Communication

Cost-efficient Clamping Solar Cells Using Candle Soot for Hole Extraction from Ambipolar Perovskite

Cite this: DOI: 10.1039/xoxxoooooox

Zhanhua Wei,[a,†] Keyou Yan,[a,†] Haining Chen,[a] Ya Yi,[b] Teng Zhang,[a] Xia Long,[a] Jinkai Li,[a] Lixia Zhang,[b] Jiannong Wang,[b,c] Shihe Yang*[,a,c]

Received ooth January 2012,
Accepted ooth January 2012

DOI: 10.1039/xoxxoooooox

www.rsc.org/

Ambient-unstable hole transporters and expensive and complicated noble metal electrode deposition are incompatible with the large scale and low-cost production of perovskite solar cells and thus would hamper their commercialization. Herein we report a new modality of perovskite solar cells that do away with the use of conventional hole transporters by directly clamping a selective hole extraction electrode made of candle soot and a deliberately engineered perovskite photoanode. The key soot/perovskite interface, which promotes hole extraction and electron blocking by forming a Schottky junction, was established seamlessly by pre-wetting and reaction embedding the carbon particles. Femtosecond time-resolved photoluminescence revealed a high hole extraction rate at 1.92 ns^{-1}. We have now achieved 11.02 % efficiency, making an important step towards roll-to-roll production of perovskite solar cells.

Organometal trihalide perovskites have stood out as a prominent light harvester for novel high efficiency solid-state solar cells.[1-22] Although the perovskites in themselves are advantageous for their solution processability and low-cost, current perovskite solar cells typically require an expensive and air-sensitive hole transporter (e.g., spiro-MeOTAD) and a noble metal electrode (Au or Ag) deposited by complicated vacuum technologies.[23,24] These drawbacks, if not adequately addressed, will hinder the industrial development and market potential of perovskite solar cells.[25] Therefore, it's highly desirable to develop alternative materials and processes that are high-performing but inexpensive, earth-abundant, environmental friendly, easily processable and energy non-intensive. As is well known, graphitic carbon, with most of the above-mentioned sought-after characteristics, has a work function of around 5.0 eV, meaning that its Fermi level is only slightly higher than the valence band edge of the perovskites.[11, 26-30] This energy band alignment probably permits the graphitic carbon to efficiently extract holes from the ambipolar perovskites,[11, 27, 31-33] an imperative step in this type of solar cells. Consequently, a suitably engineered carbon material can be up to the job with the need of neither the conventional hole transporter nor the noble metal electrode.[27-30, 34] Hitherto, however, little work has been done to develop carbon based nanomaterials in that regard to pursue cost-efficient perovskite solar cells.

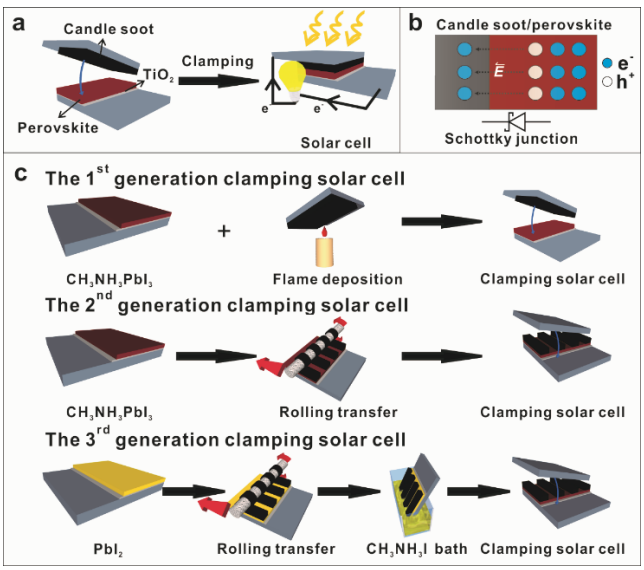

Scheme 1 | Development of candle soot/perovskite clamping solar cell. a, Conception of the clamping solar cells based on a candle soot electrode and a perovskite electrode. **b,** The putative Schottky junction formed between candle soot and perovskite, which is at the core of realizing the clamping solar cells. **c,**

(Top) Fabrication process of the 1st generation clamping solar cells by simply clamping an FTO supported candle soot film and a $CH_3NH_3PbI_3$ photoanode. (Middle) Fabrication of the 2nd generation clamping solar cells by rolling transfer assisted clamping. (Bottom) Fabrication of the 3rd generation clamping solar cells by chemically promoted rolling transfer clamping, with a CH_3NH_3I bath for the *in situ* conversion of PbI_2 to $CH_3NH_3PbI_3$ partially embedding the soot electrode.

In this work, we propose and develop the concept of clamping solar cells by joining together separately optimized perovskite photoanode and candle soot hole extraction electrode (see Scheme 1a). Candle soot is used because it is potentially a hole-extracting electrode material that is inexpensive, environmental friendly, stable and abundant. At the core of this design is the carbon/perovskite interface, which ideally should be a Schottky junction as shown in Scheme 1b. Specifically, the candle soot electrode should be able to selectively extract holes but reject electrons from the perovskite. Our systematic efforts have been centered on the optimization of the carbon/perovskite interface, as illustrated in Scheme 1c, by stepwise evolving the clamping solar cells across three generations. The 1st generation is featured by directly clamping a perovskite photoanode, to a candle soot electrode flame-deposited on FTO, producing a working cell with a decent efficiency. However, two problems were encountered: (1) the candle soot was not sufficiently conductive and (2) the uncontrollable clamping mode failed to ensure dependable contacts between the perovskite and the candle soot, resulting in large internal resistance and an inferior photovoltaic performance. To address these problems, the candle soot was annealed to enhance graphitization and thus the conductivity, and rolling transfer of the candle soot was adopted to improve the interface contact, leading to the 2nd generation clamping solar cells. Indeed, the overall solar cell performance including efficiency and reproducibility has been improved significantly. However, the fill factor and power conversion efficiency (PCE) are still unsatisfactory compared to spiro-MeOTAD based cells, probably associated with the low and non-ideal interface contacts between perovskite and candle soot. This problem is largely resolved by a dramatic leap to the 3rd generation clamping solar cells enabled by a two-step method. Now the perovskite film is fabricated by firstly depositing a PbI_2 precursor layer, immediately followed by the rolling transfer of candle soot, and finally subjecting the sample to a CH_3NH_3I bath treatment. In this chemically promoted clamping process, the *in situ* conversion of PbI_2 to $CH_3NH_3PbI_3$ conspired to yield an interpenetrating interface between perovskite and candle soot with excellent controllability. Thus the combination of such simple mechanical and chemical clamping techniques has allowed us to greatly boost the PCE (to 11.02%) as well as the performance reproducibility.

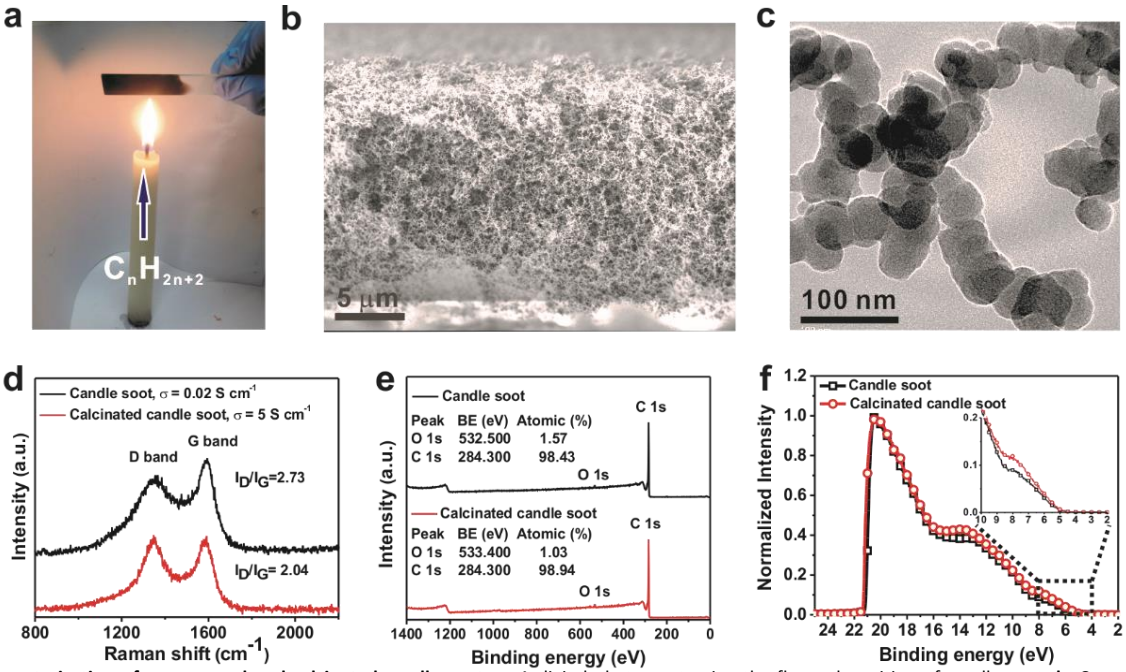

Figure 1 | Characterization of as-prepared and calcinated candle soot. a, A digital photo portraying the flame deposition of candle soot. **b,** Cross-sectional SEM image of the sponge-like candle soot film. **c,** TEM image of the as-prepared bi-continuous network of chain-like candle soot nanoparticles. **d,** Raman spectra and conductivity results of the as-prepared and the calcinated candle soot. **e,** X-ray photoelectron spectra (XPS) and **f,** Ultraviolet photoelectron spectra (UPS) of the as-prepared and the calcinated candle soot.

We start by firstly demonstrating the synthesis of candle soot and presenting some of its basic structural and electronic properties useful for the hole extraction. Figure 1a illustrates the classical flame deposition of candle soot, which is expedient for large-scale synthesis of carbon nanoparticles. By simply putting a piece of glass in the candle flame, a tens of micrometers thick film of black candle soot could be deposited in seconds. From the scanning electron microscope (SEM) image in Figure 1b, one can see that a loose sponge-like structure of the as-prepared candle soot is well assembled. The transmission electron microscope (TEM) image in Figure 1c further reveals the typical bi-continuous, branched nanochain structure, which is actually comprised of strings of 30 nm nanoparticles. The calcination at 1000 ℃ in argon gas did not cause noticeable morphology change (refer to Figure S1), but it raised the electric conductivity precipitously up to ~5 S cm^{-1}, which is two orders of magnitude higher than the as-prepared candle soot (~0.02 S cm^{-1}), due presumably to the removal of the organic residues and the improved graphitization. As expected, the Raman spectra in Figure 1d show a sharpened G

View Article Online
DOI: 10.1039/C4EE01983K
ARTICLE

band and a reduced I_D/I_G ratio arising from the calcination. In addition, the X-ray photoelectron spectra (XPS) in Figure 1e also testify that the calcinated candle soot contains a smaller concentration of oxygen (1.03 %) than the as-prepared candle soot (1.57 %). The dramatically enhanced conductivity bodes well for the interfacial charge transfer and charge transport in solar cells that use such candle soot as electrodes, as will be discussed below. The ultraviolet photoelectron spectroscopy (UPS) in Figure 1f reveals a similar work function of 5.00 eV for both the as-prepared and the calcinated candle soot, but the latter displays a higher density of states near the Fermi level (see the inset in Figure 1f) due to the improved graphitization. At any rate, the Fermi level is suitable for hole extraction from perovskite because it is only slightly higher than the valence band edge of the $CH_3NH_3PbI_3$ perovskite.

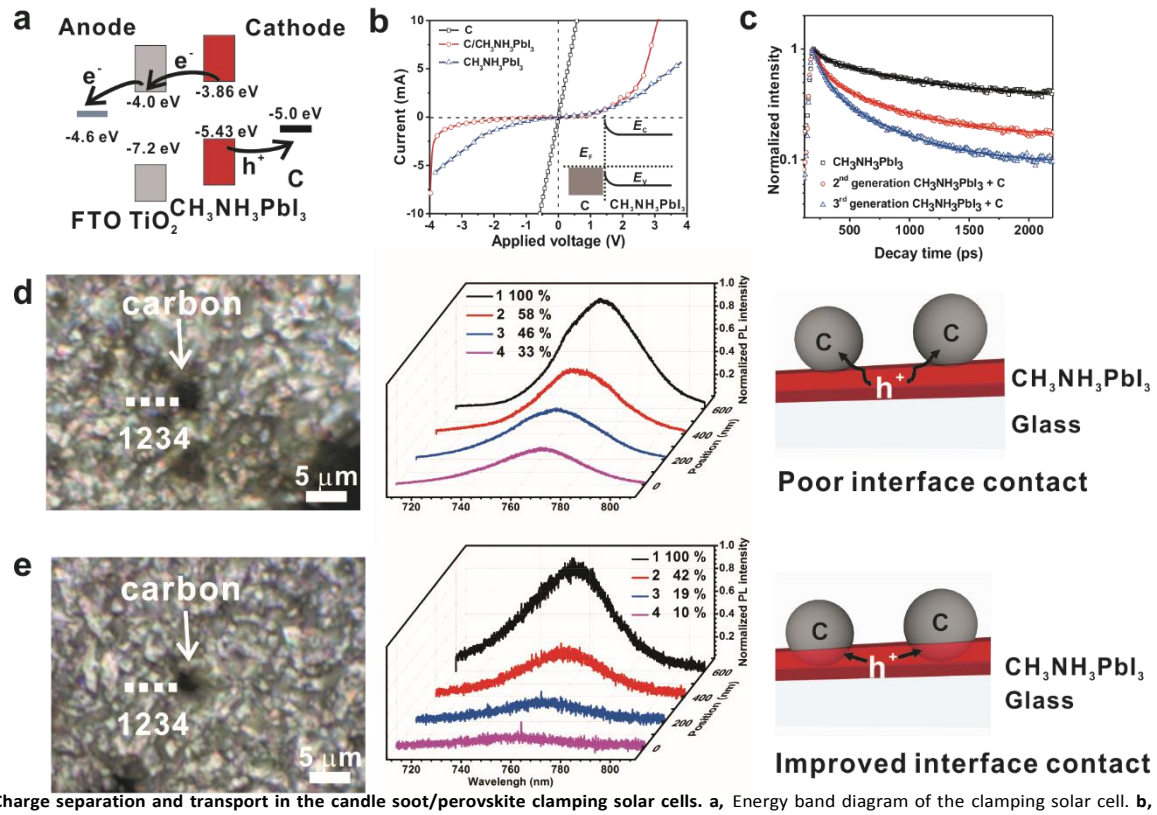

Figure 2 | Charge separation and transport in the candle soot/perovskite clamping solar cells. a, Energy band diagram of the clamping solar cell. **b,** *I-V* curves of FTO/C/FTO, FTO/$CH_3NH_3PbI_3$/FTO and FTO/C/$CH_3NH_3PbI_3$/FTO clamping devices (inset is a schematic equilibrium energy diagram of the Schottky junction of C/$CH_3NH_3PbI_3$). **c,** Time-resolved photoluminescence (PL) spectra of the as-prepared $CH_3NH_3PbI_3$, and the 2nd generation $CH_3NH_3PbI_3$ + C and the 3rd generation $CH_3NH_3PbI_3$ + C electrodes. Distance dependent PL quenching in the 2nd generation $CH_3NH_3PbI_3$ + C film **d,** and in the 3rd generation $CH_3NH_3PbI_3$ + C film **e,** The marked points in the optical microscope images in **d** and **e** are not to scale, and the actual line scanning step is 0.2 μm.

As mentioned above, the key challenge in developing the clamping solar cells lies in the optimization of charge separation and transport at the candle soot/perovskite interface. Since the 1st generation clamping cells are wide off the mark in this aspect, we focus our attention on the charge transfer behaviors in the 2nd and the 3rd generations of clamping solar cells. Figure 2a presents the energy band diagram of the clamping cells based on Figure 1f and our previous report.[26] In a working cell, after light excitation, the electron is excited up to the conduction band (CB) at -3.86 eV, injected to the CB of TiO_2 (-4.00 eV) and finally collected at FTO anode (work function: 4.70 eV). At the same time, the hole in the valance band (VB) at -5.43 eV is extracted to the candle soot electrode (work function: 5.00 eV). It follows that key to the operation of clamping cell are two selective charge extraction interfaces sandwiching the ambipolar perovskite layer. The first is the $TiO_2/CH_3NH_3PbI_3$ interface for electron extraction, which has been well established by the previous research work.[7, 10] It is the second interface of candle soot/perovskite for hole extraction that is really the linchpin of our clamping solar cells. In order to understand the nature of the candle soot/perovskite interface, we measured current-voltage (*I-V*) curves of the FTO/C/$CH_3NH_3PbI_3$/FTO device together with the two control devices of FTO/C/FTO and FTO/$CH_3NH_3PbI_3$/FTO devices, which are displayed in Figure 2b. One can see that the FTO/C/$CH_3NH_3PbI_3$/FTO device presents a rectifying characteristics of a Schottky junction. In the control measurements, the FTO/C/FTO device displays a linear *I-V* curve suggesting ohmic contact between FTO and C, while the FTO/$CH_3NH_3PbI_3$/FTO device presents a symmetric nonlinear *I-V* curve due to the semiconductive property of the perovskite. Thus the Schottky junction has been formed at the candle soot/perovskite interface, which induces a built-in field and the attendant energy band bending (inset in Figure 2b) promoting the directional hole extraction to candle soot but rejecting the electrons.

Femtosecond time-resolved photoluminescence (TRPL) was further employed to investigate the early interfacial or near interfacial carrier dynamics in the 2nd and 3rd generation $CH_3NH_3PbI_3$ + C films using the pure $CH_3NH_3PbI_3$ film as a control sample. The results are shown in Figure 2c. As usual, PL lifetimes (τ) is defined as the time it takes for the PL

intensity to fall to 1/e of its original intensity. We can see that the pure $CH_3NH_3PbI_3$ film exhibits the longest PL lifetime of 2165.7 ps, and the candle soot induced PL quenching shortens the PL lifetime of the 2nd and 3rd generation $CH_3NH_3PbI_3$ + C films to 409.2 ps and 235.4 ps, respectively. By using the relation $k_{ct}=1/\tau-1/\tau_0$, the charge transfer rate of the 3rd generation electrode is estimated to be 3.79 ns^{-1}, which is 1.91 times higher than the 2nd generation electrode. Notably, the hole extraction rate of candle soot is even comparable with that of spiro-MeOTAD,[15] which is a standard hole transport material used in perovskite solar cells. Evidently, the chemically promoted 3rd generation clamping solar cell allows more efficient hole extraction from perovskite to candle soot than the 2nd generation clamping solar cell. In order to further confirm this result, we performed nanoscale PL line scans at the single particle level on the 2nd and 3rd generation $CH_3NH_3PbI_3$ + C films, and the results are presented in Figure 2d and 2e, respectively. As shown in the left panels of Figure 2d and 2e, faceted perovskite microcrystals form continuous films, above which some carbon aggregates (black color) can be observed. By performing a line PL scan near a selected carbon aggregate along the dashed line (from point 1 to point 4, scanning step: 200 nm) with a focused laser beam, a series of PL spectra were acquired, and the corresponding PL spectra are shown in the middle panels of Figure 2d and 2e. In general, the PL intensity decreases as the laser beam is scanned towards the carbon aggregates, but the 3rd generation electrode displays a much shorter PL decay length (λ is the length taken for the PL intensity to fall to 1/e of its original intensity; shorter λ means stronger PL quenching) than the 2nd generation electrode. For instance, the candle soot in the 3rd generation film can quench at point 4 up to 90 % of the PL intensity at point 1 within 600 nm around it, whereas only ~70% PL quenching is observed in the 2nd generation film at a similar distance. This difference in distance dependent PL quenching also reflects the different hole extraction capabilities in the electrodes due to the different interfacial contacts between candle soot and perovskite. As schematically illustrated in the right panels of Figure 2d and 2e, the improved interface contact in the 3rd generation film (Figure 2e) over the 2nd generation film (Figure 2d) by the chemical promoted interpenetration between candle soot and perovskite facilitates the hole extraction and thereby quenches the PL more efficiently nearby.

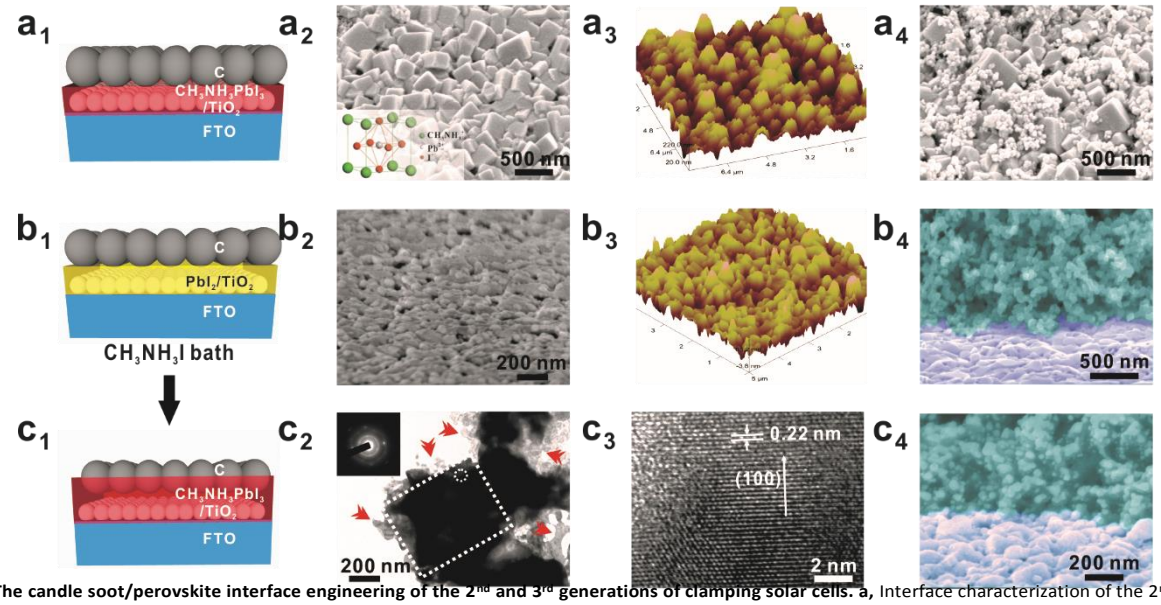

Figure 3 | The candle soot/perovskite interface engineering of the 2nd and 3rd generations of clamping solar cells. a, Interface characterization of the 2nd generation clamping solar cells: **a_1,** Schematic illustrating the interface of C/$CH_3NH_3PbI_3$. **a_2,** Tilted-view SEM and **a_3,** 3D AFM images of the pure $CH_3NH_3PbI_3$ film. **a_4,** Tilted-view SEM image of C/$CH_3NH_3PbI_3$. **b, and c,** Interface engineering of the 3rd clamping solar cells: **b_1,** Schematic illustrating the interface of C/PbI_2, **b_2,** Tilted-view SEM and **b_3,** 3D AFM images of the precursor PbI_2 film, and **b_4,** Tilted-view SEM image of the C/PbI_2 interface. **c_1,** Schematic illustrating the chemically engineered interface by *in situ* conversion from PbI_2 to $CH_3NH_3PbI_3$, partially burying C into the $CH_3NH_3PbI_3$ film, **c_2,** TEM image of C/$CH_3NH_3PbI_3$ nanoparticles (red arrow indicates free carbon nanoparticle and dashed box indicates cube-like perovskite microcrystal with some attached carbon nanoparticles; inset: selected area electron diffraction (SAED) pattern of the dashed box. **c_3,** HRTEM image (taken at the dash circle in **c_2**) of single crystalline $CH_3NH_3PbI_3$, and **c_4,** Tilted-view SEM image of the chemically engineered interface of C/$CH_3NH_3PbI_3$.

Now a closer examination at the chemically engineered soot/perovskite interfaces is in order, in an effort to expedite the technical optimization of the clamping solar cells. Figure $3a_1$ schematizes the 2nd generation physical contact between C/$CH_3NH_3PbI_3$, in which candle soot is press attached to the perovskite photoanode. The SEM image in Figure $3a_2$ reveals perovskite crystals in the tetragonal system (inset of Figure $3a_2$) with a cuboid-shaped morphology, resulting in a rough top surface (for more characterization results of perovskite-related thin film, see Figure S2). This rough characteristic of the top surface is seen more clearly from the 3D height profile atomic force microscope (AFM) image in Figure $3a_3$. Indeed, the top surface of the $CH_3NH_3PbI_3$ film is full of convex-concave features spanning a tens of nanometer range, which are useful for the subsequent filling of size- and morphology-matched carbon soot nanoparticles, as shown in Figure $3a_4$. This surface feature is particularly beneficial to the mechanical clamping in the 1st generation clamping solar cells, which owe their initial success precisely to the rough perovskite surface.

Figure 3b and 3c feature the chemically promoted interface engineering in the 3rd generation clamping solar cells. The key process lies in the *in situ* conversion of PbI_2 to $CH_3NH_3PbI_3$ and chemical embedding of C into $CH_3NH_3PbI_3$ at the interface, as schematically illustrated in Figure $3b_1$ and $3c_1$. Compared to the above-described perovskite crystals (Figure $3a_1$), the precursor PbI_2 has even smaller particle sizes (~200 nm) (Figure $3b_2$) and

View Article Online
DOI: 10.1039/C4EE01983K
ARTICLE

yields smaller but sharper surface features (Figure 3b$_3$), permitting more interpenetrating contacts between C and PbI_2. Most importantly, these pre-configured contacts will allow the subsequent *in situ* conversion of PbI_2 to $CH_3NH_3PbI_3$ to greatly improve the interface and lower the barrier to charge transfer. As schematized in Figure 3c$_1$, the $CH_3NH_3PbI_3$ precursors could penetrate into and wrap around the mesoporous candle soot and crystallize, holding together the soot particles and thereby proffering a high-quality interface for facile hole extraction. This chemical embedding effect was caught by careful TEM observations (see below and Figure S3). As shown in Figure 3c$_2$, part of the candle soot network becomes embedded in the perovskite crystal film after *in situ* conversion (see the edge of dashed box) and the candle soot particles conglutinated by perovskite are still noticeable around the big microcrystals (see red arrays and supporting information). The selective area electron diffraction (SAED) pattern gives further evidence of the chemical embedment. As shown in the inset of Figure 3c$_2$ (taken from the dashed box), the ring and dotted patterns are indexed to the graphitic carbon nanoparticles and the perovskite microcrystals separately, in agreement with the fact that the candle soot is really embedded into the perovskite (also see the Figure S3). The HRTEM in Figure 3c$_3$ demonstrates the high crystallinity of the perovskite grown (it appears to grow by filling the pores in the candle soot network) in mesoporous candle soot judging from the directional lattice fringes ascribable to the (100) plane (d = 0.22 nm), which seem to be uninterrupted by the intervening soot nanoparticles. The SEM image in Figure 3c$_4$ manifests that the chemically engineering has filled the interstitial regions of the candle soot with perovskite at least near the interface ensuring the interpenetration conducive to the efficient charge separation. Of note, the pre-wetting and the preconditioning of the carbon surface in the step of CH_3NH_3I bath soaking and ensuing crystallization has also played a large role in securing such an interpenetrating interface.

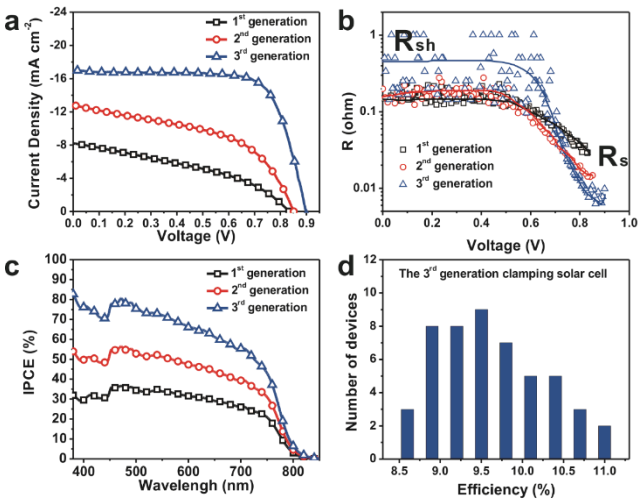

Figure 4 | Performance characteristics of the three generation clamping solar cells. a, *J-V* curves of the three generations of clamping solar cells showing an increasing PCE as a result from the interface engineering. **b,** *R-V* curves of the three generations of solar cells derived from the corresponding *J-V* curves. **c,** IPCE curves of the three generations of clamping solar cells. **d,** PCE histograms of the 3rd generation clamping solar cells obtained from the measurements of 50 devices.

After gaining a clear picture about the structural and electronic characteristics of the engineered interfaces of candle soot/perovskite, we now compare the performance of the three generations of clamping solar cells fabricated by direct clamping, rolling-transfer clamping and chemically promoted clamping, respectively. Figure 4a presents the current density-voltage (*J-V*) curves and the relevant performance parameters are summarized in Table 1. The result underscores the progressive interface engineering efforts that have made the clamping solar cells more and more efficient from generation to generation, evolving into the final high-performing device. Even though the 1st generation solar cells are made by the direct clamping, it still achieves V_{oc} of 0.83 V, J_{sc} of 8.23 mA cm^{-2} and FF of 0.38, amounting to a 2.60 % PCE. The bottlenecks are the inferior J_{sc} and FF, most probably arising from the existing contact blind points between candle soot and perovskite conceivable for a simple mechanical joint. In the 2nd generation, The J_{sc} is increased to 12.8 mA cm^{-2}, FF to 0.50 and V_{oc} to 0.85 V, yielding an impressively enhanced PCE of 5.44 %. Two contributing factors can be considered for this performance enhancement. Firstly, the conductivity of candle soot has been significantly enhanced through calcination as has been mentioned above. Secondly, rolling transfer technique has considerably compacted the candle soot carbon electrode to further lower the electric resistance and to encourage the intimate contacts with the perovskite. Although involving more control than the direct clamping mode, the rolling transfer technique is also viable for large scale production. At last, it is the chemical promotion strategy that has evolved the clamping solar cells to the best-performing 3rd generation with a V_{oc} of 0.90 V, J_{sc} of 17.00 mA cm^{-2} and FF of 0.72, yielding an overall PCE of 11.02 %. Equally impressive is the cell stability; after storage for over one month without encapsulation and special protection, the cell still retained >85% of the initial measured efficiency and there is no loss of J_{sc} at all (Figure S4). In principle, V_{oc} and FF are related to the shunt resistance (R_{sh}) and series resistance (R_s) according to the standard equivalent diode circuit model of solar cells. From the derivative of the $J-V$ curves, the resistances can be estimated through the equation $R = -(dJ/dV)^{-1}$, and the resulting resistance-voltage (*R-V*) curves are shown in Figure 4b for all of the three generation solar cells. It can be seen that R_s decreases whereas R_{sh} increases from generation to generation, in association with the improved FF and V_{oc} resulting from the increasing sophistication of the interface engineering. To best our knowledge, this is the highest efficiency among hole transporter-free and Au-free perovskite solar cells. For the sake of direct comparison, an Au cathode sputtering deposited on an FTO/TiO_2/$CH_3NH_3PbI_3$ film obtained a PCE of 4.90 % (Figure S5), while a graphite plates/perovskite clamping solar cell exhibited a PCE of 0.99 % (Figure S6).

Table 1 Performance summary of the three generation clamping solar cells.

Solar cell	Voc (V)	Jsc (mA cm^{-2})	FF	PCE (%)	Best-PCE (%)
1st generation	0.81± 0.02	7.15± 1.08	0.28± 0.10	1.73±0.87	2.60
2nd generation	0.84± 0.01	11.75± 1.04	0.46± 0.04	4.56±0.88	5.44
3rd generation	0.88± 0.02	16.50± 0.52	0.67± 0.05	9.78±1.24	11.02

The incident photon-to-electron conversion efficiency (IPCE) spectra specify the ratio of extracted current to incident photons at a given wavelength. Figure 4c presents the corresponding IPCE curves of the above three generations of clamping solar cells. Obviously, the resultant IPCEs generally increase in the order of the 1st generation < 2nd generation < 3rd generation, in concordance with the J_{sc} order. Similarly, all of the three generation clamping solar cell show a good photon-to-electricity conversion ability in blue and green light region (< 600 nm) but poor conversion capacity in the red light region (600 nm – 800 nm), linear decreasing from 740 nm and cut off at 800 nm, the lower IPCE value at longer wavelengths (> 700 nm) is attributed to the poor absorbance ability in this region (refer to Figure S2a), which is consistent with previous spiro-MeOTAD based perovskite solar cell.[3, 6, 35] Integration of the products of the AM 1.5G photon flux with a given IPCE spectrum yields a predicted J_{sc} of 7.56 mA cm^{-2}, 11.51 mA cm^{-2} and 16.30 mA cm^{-2} for the 1st, 2nd and 3rd generation of clamping solar cells, respectively, in excellent agreement with the *J-V* results. In order to investigate the reproducibility of the 3rd generation clamping solar cell, 50 separate devices were fabricated and tested, histograms of the cell-performance PCE is presented in Figure 4d. As can be seen form the results, the average PCE located at about 9.63 %, while the lowest efficiency is 8.60 % and the highest efficiency is 11.02 %. In general, after the development of three generation candle soot/perovskite solar cell, we can achieve a relatively high PCE up to 11.02 % with good reproducibility.

Conclusions

To sum up, we have established a cost-efficient, environmentally stable and abundant candle soot as an efficient hole extractor and developed a concept of clamping solar cells by judiciously interfacing the candle soot with $CH_3NH_3PbI_3$ films. In this effort, three generations of clamping solar cells were evolved from direct clamping to rolling-transfer clamping and to chemically promoted clamping accelerated by the mechanistic understanding of inner workings. Up to this stage, the third generation clamping solar cells have already achieved a remarkable efficiency of 11.02 % and good long term stability. Femtosecond time resolved PL and distance dependent PL measurements have confirmed the conclusion that the improved PCE is largely due to the enhanced directional hole extraction at the candle soot/perovskite interface through the mechanical and chemical promotion strategies. Thus we have shown that the clamping solar cells represent a new type of easily processable but high performing photovoltaic devices. The present work has not only promoted the fundamental understanding on the clamping cell working mechanisms but also made great headway towards roll-to-roll production and realistic commercialization of perovskite solar cells.

Experimental

Materials Preparation. FTO-candle soot film was directly deposited by putting a FTO glass in the candle flame for about 1 min. Black candle soot powder was collected by putting a glass in the candle flame and scrapping the powder off. The soot powder was further calcinated at 1000 °C in argon gas. To prepare candle soot solid tape, calcinated candle soot was dispersed in ethanol to make a slurry (10 wt%) firstly, the obtained slurry was then pasted on a Cu foil and dried at 80 °C for 10 min to obtain a carbon tape.

Solar cell device fabrication. Firstly, FTO/compact TiO_2/mesoporous TiO_2/PbI_2 substrates were prepared according a procedure reported previously with slight modifications (for details, refer to supporting information).[6, 36] For the 1st and 2nd generation clamping solar cells, the substrates were soaked into a CH_3NH_3I bath to get a $CH_3NH_3PbI_3$ film. A piece of FTO-candle soot film and the $CH_3NH_3PbI_3$ film were directly clamped to make the 1st generation clamping solar cells. For the 2nd generation clamping solar cells, a calcinated carbon soot electrode about 10 μm thick was rolling transferred onto the $CH_3NH_3PbI_3$ film using the as-prepared carbon tape with a home-made rolling transfer equipment (the compression pressure is estimated to be about 10 MPa). Then another piece of FTO glass was clamped to the $CH_3NH_3PbI_3$/C film. After rolling transfer, the calcinated candle soot thin film was strongly attached onto the perovskite film and did not peel off even after purging with compressed air. In the case of the 3rd generation clamping solar cells, the calcinated candle soot electrode was rolling transferred onto the PbI_2 film before CH_3NH_3I bath treatment, and other procedures were similar to the 2nd generation clamping solar cell fabrication process.

Acknowledgements

This work was supported by the HK-RGC General Research Funds (GRE No. HKUST 606511, 605710, 604410).

Notes and references

[a] Department of Chemistry, [b] Department of Physics, [c]William Mong Institute of Nano Science and Technology, The Hong Kong University of Science and Technology, Clear Water Bay, Kowloon, Hong Kong, China
*Corresponding email: chsyang@ust.hk
† These authors contributed equally to this work.

Note added IN PROOF: During the revision of this paper, a highly relevant article on this topic was published: A. Mei, X. Li, L. Liu, Z. Ku, T. Liu, Y. Rong, M. Xu, M. Hu, J. Chen, Y. Yang, M. Grätzel and H. Han, *Science*, 2014, **345**, 295-298.

Electronic Supplementary Information (ESI) available: Experimental details, Figure S1-S10 and Table S1. See DOI: 10.1039/b000000x/

1. O. Malinkiewicz, A. Yella, Y. H. Lee, G. M. Espallargas, M. Graetzel, M. K. Nazeeruddin and H. J. Bolink, *Nat. Photon.*, 2013, **8**, 128-132.
2. M. Z. Liu, M. B. Johnston and H. J. Snaith, *Nature*, 2013, **501**, 395-398.
3. D. Liu and T. L. Kelly, *Nat. Photon.*, 2013, **8**, 133-138.
4. J. H. Heo, S. H. Im, J. H. Noh, T. N. Mandal, C.-S. Lim, J. A. Chang, Y. H. Lee, H.-j. Kim, A. Sarkar, M. K. Nazeeruddin, M. Grätzel and S. I. Seok, *Nat. Photon.*, 2013, **7**, 486-491.
5. Q. Chen, H. Zhou, Z. Hong, S. Luo, H.-S. Duan, H.-H. Wang, Y. Liu, G. Li and Y. Yang, *J. Am. Chem. Soc.*, 2013, **136**, 622-625.
6. J. Burschka, N. Pellet, S. J. Moon, R. Humphry-Baker, P. Gao, M. K. Nazeeruddin and M. Gratzel, *Nature*, 2013, **499**, 316-318.
7. M. M. Lee, J. Teuscher, T. Miyasaka, T. N. Murakami and H. J. Snaith, *Science*, 2012, **338**, 643-647.

View Article Online
DOI: 10.1039/C4EE01983K

8. H. S. Kim, C. R. Lee, J. H. Im, K. B. Lee, T. Moehl, A. Marchioro, S. J. Moon, R. Humphry-Baker, J. H. Yum, J. E. Moser, M. Gratzel and N. G. Park, *Sci. Rep.*, 2012, **2**, 591-598.
9. J. H. Im, C. R. Lee, J. W. Lee, S. W. Park and N. G. Park, *Nanoscale*, 2011, **3**, 4088-4093.
10. A. Marchioro, J. Teuscher, D. Friedrich, M. Kunst, R. van de Krol, T. Moehl, M. Gratzel and J. E. Moser, *Nat. Photon.*, 2014, **8**, 250-255.
11. E. Edri, S. Kirmayer, A. Henning, S. Mukhopadhyay, K. Gartsman, Y. Rosenwaks, G. Hodes and D. Cahen, *Nano. Let.t*, 2014, **14**, 1000-1004.
12. S. D. Stranks, G. E. Eperon, G. Grancini, C. Menelaou, M. J. P. Alcocer, T. Leijtens, L. M. Herz, A. Petrozza and H. J. Snaith, *Science*, 2013, **342**, 341-344.
13. J. You, Z. Hong, Y. Yang, Q. Chen, M. Cai, T.-B. Song, C.-C. Chen, S. Lu, Y. Liu, H. Zhou and Y. Yang, *ACS Nano*, 2014, **8**, 1674-1680.
14. A. Yella, L.-P. Heiniger, P. Gao, M. K. Nazeeruddin and M. Grätzel, *Nano. Lett.*, 2014, **14**, 2591-2596.
15. G. C. Xing, N. Mathews, S. Y. Sun, S. S. Lim, Y. M. Lam, M. Gratzel, S. Mhaisalkar and T. C. Sum, *Science*, 2013, **342**, 344-347.
16. J. A. Christians, R. C. Fung and P. V. Kamat, *J. Am. Chem. Soc.*, 2014, **136**, 758-764.
17. A. Kojima, K. Teshima, Y. Shirai and T. Miyasaka, *J. Am. Chem. Soc.*, 2009, **131**, 6050-6051.
18. J. M. Ball, M. M. Lee, A. Hey and H. J. Snaith, *Energy & Environmental Science*, 2013, **6**, 1739-1743.
19. B. Cai, Y. Xing, Z. Yang, W.-H. Zhang and J. Qiu, *Energy & Environmental Science*, 2013, **6**, 1480-1485.
20. G. E. Eperon, S. D. Stranks, C. Menelaou, M. B. Johnston, L. Herz and H. Snaith, *Energy & Environmental Science*, 2014, **7**, 982-988.
21. K. Wojciechowski, M. Saliba, T. Leijtens, A. Abate and H. J. Snaith, *Energy & Environmental Science*, 2014, **7**, 1142-1147.
22. P. Gao, M. Grätzel and M. K. Nazeeruddin, *Energy & Environmental Science*, 2014, **7**, 2448-2463.
23. P. Qin, S. Tanaka, S. Ito, N. Tetreault, K. Manabe, H. Nishino, M. K. Nazeeruddin and M. Gratzel, *Nat. Commun.*, 2014, **5**, 3834-3840.
24. Y. S. Kwon, J. Lim, H.-J. Yun, Y.-H. Kim and T. Park, *Energy & Environmental Science*, 2014, **7**, 1454-1460.
25. G. Hodes, *Science*, 2013, **342**, 317-318.
26. J. Qiu, Y. Qiu, K. Yan, M. Zhong, C. Mu, H. Yan and S. Yang, *Nanoscale*, 2013, **5**, 3245-3248.
27. Z. Ku, Y. Rong, M. Xu, T. Liu and H. Han, *Sci. Rep.*, 2013, **3**, 3132-3137.
28. Y. Rong, Z. Ku, A. Mei, T. Liu, M. Xu, S. Ko, X. Li and H. Han, *The Journal of Physical Chemistry Letters*, 2014, **5**, 2160-2164.
29. H. Han, M. Xu, Y. Rong, Z. Ku, A. Mei, T. Liu and L. Zhang, *J. Mater. Chem. A*, 2014, **2**, 8607-8611.
30. Z. Li, S. A. Kulkarni, P. P. Boix, E. Shi, A. Cao, K. Fu, S. K. Batabyal, J. Zhang, Q. Xiong, L. H. Wong, N. Mathews and S. G. Mhaisalkar, *ACS Nano*, 2014, **8**, 6797-6804.
31. W. A. Laban and L. Etgar, *Energy & Environmental Science*, 2013, **6**, 3249-3253.
32. J. J. Shi, J. Dong, S. T. Lv, Y. Z. Xu, L. F. Zhu, J. Y. Xiao, X. Xu, H. J. Wu, D. M. Li, Y. H. Luo and Q. B. Meng, *Appl. Phys. Lett.*, 2014, **104**, 063901-063905.
33. L. Etgar, P. Gao, Z. S. Xue, Q. Peng, A. K. Chandiran, B. Liu, M. K. Nazeeruddin and M. Gratzel, *J. Am. Chem. Soc.*, 2012, **134**, 17396-17399.
34. A. Mei, X. Li, L. Liu, Z. Ku, T. Liu, Y. Rong, M. Xu, M. Hu, J. Chen, Y. Yang, M. Grätzel and H. Han, *Science*, 2014, **345**, 295-298.
35. W. Yuan, H. Zhao, H. Y. Hu, S. Wang and G. L. Baker, *Acs. Appl. Mater. Inter.*, 2013, **5**, 4155-4161.
36. Z. Zhu, J. Ma, Z. Wang, C. Mu, Z. Fan, L. Du, Y. Bai, L. Fan, H. Yan, D. L. Phillips and S. Yang, *J. Am. Chem. Soc.*, 2014, **136**, 3760-3763.

View Article Online
DOI: 10.1039/C4EE01983K

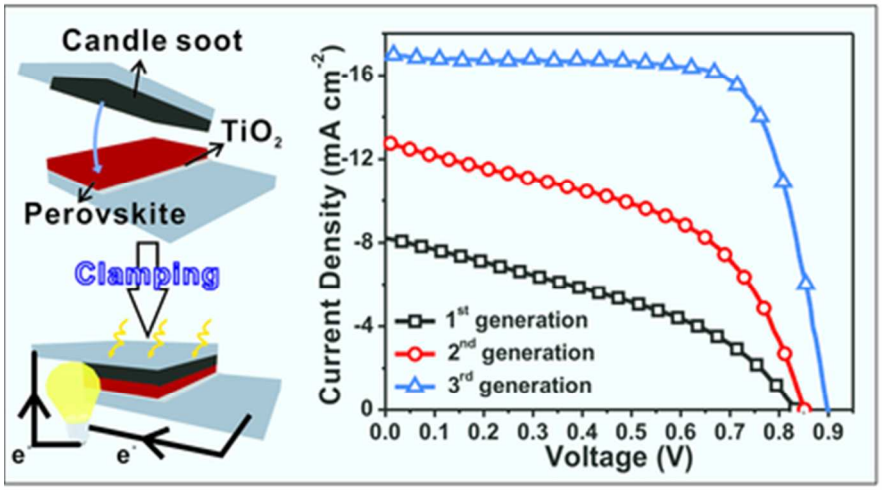

39x22mm (300 x 300 DPI)